International Journal for Modern Trends in Science and Technology, 8(09): 270-277, 2022

ISSN: 2455-3778 online
DOI: https://doi.org/10.46501/IJMTST0809051
Available online at: http://www.ijmtst.com/vol8issue09.html

Active and Reactive Power Control for PV based Single-Phase Electric Springs

B. Shanmukha Mahesh Babu[1] | Dr. R S Srinivas[2]

[1]PG Scholar, Department of EEE, Acharya Nagarjuna University, Guntur, India.
[2]Assistant Professor, Department of EEE, Acharya Nagarjuna University, Guntur, India.
Corresponding Author : rssrinivasanu@gmail.com

To Cite this Article
B. Shanmukha Mahesh Babu and Dr. R S Srinivas. Active and Reactive Power Control for PV based Single-Phase Electric Springs. International Journal for Modern Trends in Science and Technology 2022, 8(09), pp. 270-277. https://doi.org/10.46501/IJMTST0809051

Article Info
Received: 30 August 2022; Accepted: 17 September 2022; Published: 22 September 2022.

ABSTRACT

This paper proposes a simple power control for the grid connected PV system, single-phase electric springs (ES-2), that overcomes the shortcomings of the existing ES control methods. By the proposed control, the unpredictable power generated from RESs is divided into two parts, i.e. the one absorbed by the ES-2 that still varies and the other injected into the grid that turns to be controllable, by a simple and accurate signal manipulation that works both at steady-state and during RES transients. In the paper, the conventional PI and ANN controllers are proposed to control the system active powers under power variation method and voltage variation techniques. Its effectiveness is at first validated by simulations and then by experiments. To this purpose, a typical RES application is considered, and an experimental setup is arranged, built up around an ES-2 implementing the proposed control.

KEYWORDS: Electric spring, smart load, PV System, Power Control, RCD Control, DG System and ANN Controller.

1. INTRODUCTION

To meet the demand for power over the past ten years, fossil fuel facilities utilising coal, gas, and petroleum have been crucial. However, the main issue with these plants is that they could contribute to pollution, global warming, and the release of carbon dioxide, which is bad for both people and plants. Power plants in renewable energy systems hold the key to solving these issues. The most dependable DG systems are solar and wind power since they are abundant in nature, highly efficient, and reasonably priced [1].

The voltage levels are increased using a traditional Dc-Dc converter after the output of the PV system to match the demands. To produce the duty cycle needed for the PV system's dc-dc converter, a cuckoo MPPT controller is used [2]. The reliability of the PV system is increased by this combination. Using a PWM-based three phase inverter, the converter's dc output is transformed into ac. The suggested PV system is connected to grid systems in the second stage in order to run the load applications. Three phase inverters were used to synchronize these two converters.

Different load conditions are operated by this hybrid PV system that is connected to the grid. Problems with power quality are mostly affected by this variety in load changes. Voltage and current quality issues could be the cause of these issues [3]. This work focuses on balancing harmonics in system currents caused by use of load variations in order to improve power quality. A unique power device was added to the grid-connected DG system to address these issues. And also, this paper concentrates to improve the reactive power compensation in hybrid system using synchronous condenser. The main causes for these problems are load changes, system behavior or external fault conditions [4]. The control strategy for this compensation is implemented using the reference signals of reference power and calculated power. In addition, with this paper also focuses on application of Bull Optimization controller to condenser to get better control action [5]. BOA is one of the Optimization controllers have without mathematical analysis, reliable operation, fast response and generates accurate output.

The proposed system is implemented in MATLAB simulink using transfer function analysis under conventional PI controller and ANN controllers and verified the test result.

2. OPERATING PRINCIPLES OF ES-2

A. *ES-2 Topology*

As explained electric loads are divided into two types, namely CLs and NCLs. ES is an electrical device that is able to regulate the CL voltage at a pre-set value while passing the voltage (and power) fluctuations from the sources to NCL.

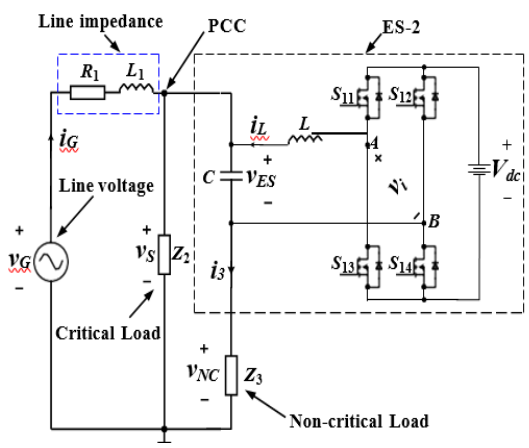

Figure. 1 Topology of ES-2 and associated circuitry.

The topology of ES-2 and the associated circuitry are drawn in Fig.1. In this figure, ES-2 is enclosed by the dashed line and consists of a single-phase voltage source inverter (VSI), an L filter and a capacitor whose voltage sums up to that of the NCL. Moreover, Z_2 is the CL, Z_3 is the NCL, v_G represents the line voltage of the power system with RESs, R_1 and L_1 are the line resistance and inductance, respectively. The branch including v_G and the line impedance supplies CL and SL. v_S denotes the voltage of point of common coupling (PCC), which is also the CL voltage.

B. *PV System Mathematical Analysis:*

One of the most dependable sources of renewable energy is the solar system. The solar system uses the sun's temperature and irradiance to produce electrical energy. An electric current run in the solar panel when the radiation explores the surface due to the photon effect. PV current is mathematically represented by the expression.

$$I_{solar} = I_{ph} - I_D - I_{sh}$$

$$I_{solar} = I_{ph} - I_o[e^{(\frac{qV_D}{nKT})}] - (\frac{V_D}{R_s})$$

Figure 2 illustrates the conversion of solar current to PV voltage using a solar electric equivalent circuit. The biggest drawback of this solar system is how challenging it is to obtain consistent sun energy. In this study, a dc-dc converter is suggested to keep the solar voltage constant [9–10]. To extract the most power possible from the PV system, an MPPT approach is used for the boost converter.

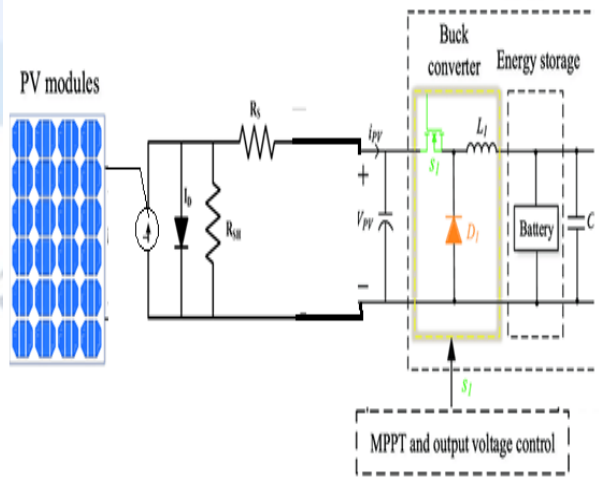

Figure 2: Solar DG System with MPPT based DC-DC converter

C. *Power Control of Existing ES-2*

The RCD control diagram for ES-2 is drawn in Figure 3. The ES voltage is here decomposed into two directions, named the radial and chordal ones. The PCC voltage is regulated by adjusting the apparent power absorbed by SL using the radial control whilst the power angle of SL is regulated at the pre-set value by the chordal control. This feature makes the SL smart as it allows ES-2 to achieve independent control of the apparent power and the power angle of SL. From this perspective, it follows that the RCD control aims at the power control of SL.

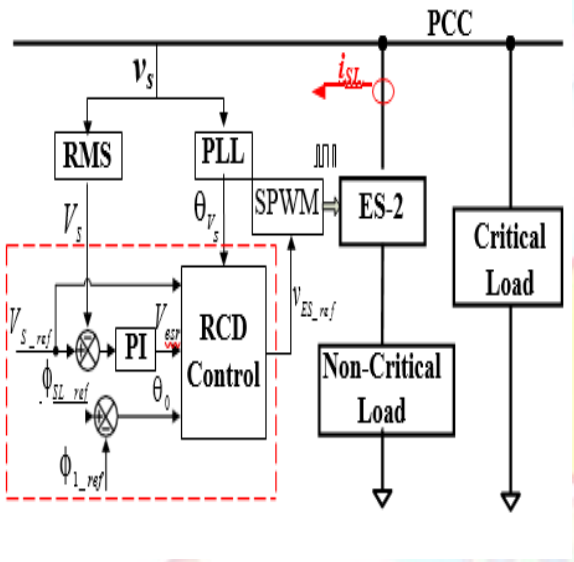

Figure 3: ES-2 control diagrams for RCD control

Although it is not like the δ control that needs almost all the circuitry parameters, impedance angle of NCL must be known in advance. It is also very difficult to operate ES-2 at pure reactive power compensation mode.

D. Requirements for the Proposed Power Control

Further to the analysis above, it would be desirable to dispose of a new power control method with the following requirements:

- No need to detect the information of grid voltage which is a far away from PCC, like δ control
- Need to decouple the control loop of the input active power from that of the PCC voltage or of the input reactive power
- By Implementing the ANN Technique to the controller, it is Easy to implement and less computational burden to get Accurate outputs as compared to other techniques.

3. THE PROPOSED CONTROL

In this section, the proposed power control is presented, explaining its ability to achieve a simple active and reactive power control for ES-2 by a local signal manipulation. In the proposed control, the single-phase *dq* rotating frame is adopted

A. *Active and Reactive Power of ES System*

Active and Reactive Power of ES System The sinusoidal voltage vS(t) and current i1(t) can be expressed as

$$v_s(t) = \sqrt{2} V_s \cos(\omega t + \phi) \quad (1)$$

$$i_s(t) = \sqrt{2} I_1 \cos(\omega t + \psi) \quad (2)$$

where φ and ψ are the initial phases, ω is the angular frequency, VS and I1 denote the rms value of vS(t) and i1(t), respectively. By looking from PCC to the right side in Fig. 1, active, reactive and apparent powers can be expressed from (3) to (5), where Pin and Qin are the total active and reactive power absorbed by ES, CL and NCL together, respectively; S ~ denotes the apparent power

S =Vs. Ǐ1s*

$$= V_s I_1 [\cos(\phi - \psi) + j \sin(\phi - \psi) \quad (3)$$

$$= P_{in} + j\, Q_{in} \quad (4)$$

Where

$$P_{in} = V_s I_1 [\cos(\phi - \psi) \quad (5)$$

$$Q_{in} = V_s I_1 \sin(\phi - \psi) \quad (5)$$

According to [19], the active and reactive powers can be represented in terms of the variables on a rotating frame as

$$P_{in} = v_d\, i_d + v_q\, i_q \quad (6)$$

$$Q_{in} = v_d\, i_d - v_q\, i_q \quad (7)$$

where vd and vq are the components of vS in the dq rotating frame. The same analogy applies to id and iq. If the voltage vector of vS is aligned along the d-axis of the rotating frame, (6) and (7) can be rewritten as

$$P_{in} = v_d\, i_d \quad (8)$$

$$Q_{in} = - v_d\, i_q$$

It should be remarked that (6) to (9) are used to explain the minus sign of the power control loops. It can be seen from (8) and (9) that the polarities of Pin and Qin are different. By [19], Qinref should be entered on the minus side and Pinref on the plus side.

However, the input current in Fig. 3(a) is selected to have a direction opposite to that of grid-connected converter (GCC) in [19]. As a result, the positions of the active and reactive powers, and the relevant references are exchanged in Fig. 3(a) with respect to [19]. This is due to the direction chosen for the input current in Fig. 3(a).

The calculation of Pin and Qin is detailed in Fig. 3(b), where the Fourier Transforms are used to extract the peak values and the phase angles from the detected quantities of vS and i1. One can readily recognize that (4) and (5) underlie the diagram of Fig. 3(b).

The matrix for the transformation of a vector from the αβ stationary frame to a dq rotating frame and its inverse are expressed as

$$T(\hat{\theta}) = \begin{bmatrix} \cos\hat{\theta} & \sin\hat{\theta} \\ -\sin\hat{\theta} & \cos\hat{\theta} \end{bmatrix} \quad (10)$$

$$T(\hat{\theta})^{-1} = \begin{bmatrix} \cos\hat{\theta} & -\sin\hat{\theta} \\ \sin\hat{\theta} & \cos\hat{\theta} \end{bmatrix} \quad (11)$$

Where θ ˆ is the instantaneous phase of the PCC voltage detected by a phase locked loop (PLL) block.

B. *Power Control of ES-2*

The control diagram of the proposed simple power control is shown in the block of Figure 4, enclosed by the dashed line. The control calls for the detection of variables such as the input current i_1 and the CL voltage v_S. The input active and reactive powers of the ES system, marked as P_{in} and Q_{in}, are obtained by manipulating the instantaneous values of Vs and i1 as illustrated[1].

The powers Pin and Qin are controlled by separate PI regulators. Specifically, the regulator in the d-axis controls Pin and that one in the q-axis controls Qin. Alternatively, if the control objective is the CL voltage instead of Qin, a loop outer the q-axis is added closed with a PI regulator, and its output represents the reference for Qin, designated as Qinref.

The output signals of the PI regulators in both the loops are processed through the inverse dq-to-αβ transformation to get the modulation signal vcomp1.

It should be noticed that functionality of harmonic suppression is added in Fig.4(a) by subtracting the harmonic component denoted as vS_h from vcomp1. The drive signals for the VSI transistors are obtained by the SPWM technique, just after a limiter.

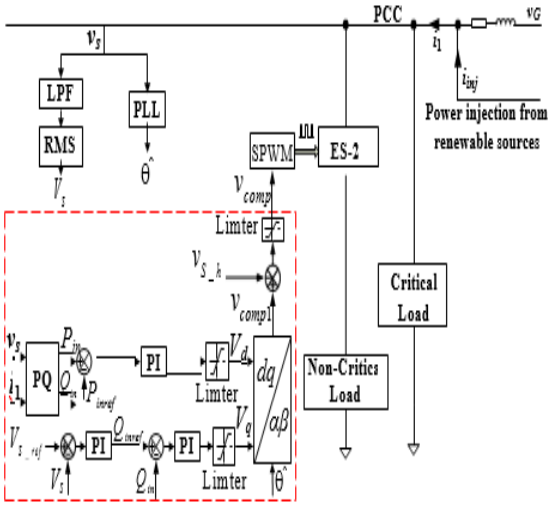

Figure 4(a): The proposed power control of ES-2

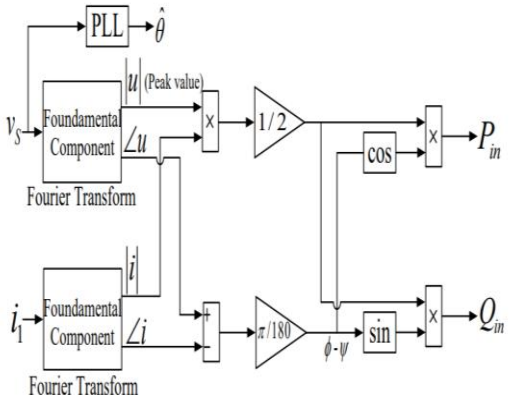

Figure 4(b) Control diagram and Calculation diagram of active and reactive power

C. *Artificial Neural Networks*

Figure 6 shows the basic architecture of artificial neural network, in which an hidden layer is indicated by circle, an adaptive node is represented by square. In this structure hidden layers are presented in between input and output layer, these nodes are functioning as membership functions and the rules obtained based on the if-then statements is eliminated. For simplicity, we considering the examined ANN have two inputs and one output. In this network, each neuron and each element of the input vector p are connected with weight matrix W.

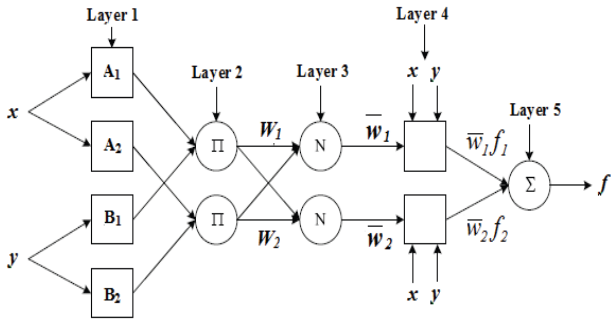

Figure 5: ANN architecture for a two-input multi-layer network

Where the two crisp inputs are x and y, the linguistic variables associated with the node function are Ai and Bi. The system has a total of five layers are shown in Figure 5.

Step by step procedure for implementing ANN:

1. Identify the number of input and outputs in the normalized manner in the range of 0-1.
2. Assume number of input stages.
3. Identify number of hidden layers.
4. By using transig and poslin commands create a feed forward network.
5. Assume the learning rate should be 0.02.
6. Choose the number of iterations.
7. Choose goal and train the system.
9. Generate the simulation block by using 'genism' command.

4. SIMULATION ANALYSIS AND RESULT

To verify the aforementioned analysis, simulations are conducted using Matlab/Simulink based on parameters shown in Table I.

Items	Values
Regulated PCC voltage (V_S)	220V
DC bus voltage (V_{dc})	400V
Line resistance (R_1)	0.1Ω
Line inductance (L_1)	2.4mH
Critical load (R_2)	43.5Ω
Non-critical load (R_3)	2.2Ω
Inductance of low-pass filter (L)	3mH
Capacitance of low-pass filter (C)	50μF

Table 1: Operating Parameters for simulation Circuit

To simplify the analysis, both CL and NCL are chosen of resistive types. It should be noticed that they can be any other linear types. For the ES-2 system under simulation, the control objectives are formulated as follows: i) RMS value of the PCC voltage or input reactive power is regulated at a pre-set values, and ii) input active power P_{in} tracks the pre-set value P_{inref}.

Two situations are investigated, namely

- P_{inref} varies at fixed V_G
- V_G varies at fixed P_{inref}

The Simulation analysis are executed in three steps. The first step is intended to verify the operation of the ES-2 when implementing the proposed control and is performed by switching off both S1 and S2. The second step is intended to check the behavior of the GCC in emulating the power injection from a RES and is performed by switching on both S1 and S2. The third step is intended to jointly debug both the ES-2 and the GCC to validate the effectiveness of the power control in a real application and is performed by switching S1 off and S2 on.

Case 1: Input Active Power Variation with Conventional PI controller and ANN controller

In this part, the value is selected for V_G to monitor its behavior when P_{inref} varies. Figure 6 shows the simulation results when P_{inref} varies. In each subfigure, two channels are recorded, reporting V_G, P_{inref}, P_{in} and RMS value of the C_L voltage, respectively,by using PI and ANN controllers with comparisons has been shown.

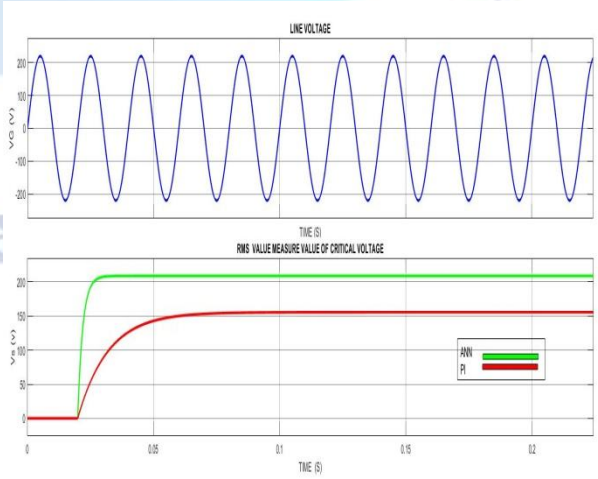

Figure 6: Simulation Waveform for input RMS value of Critical Voltage with PI and ANN Controller

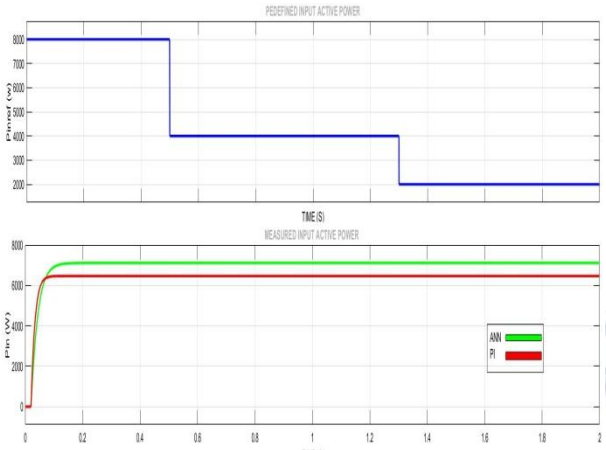

Figure 7: Simulation Waveform for Predefined and Measured Active Powers with PI and ANN Controller here from 8kw to 2kwnand then back to1.6kw @VG=230v

Figure 8: Simulation Waveform for Reactive powers of ES system with PI and ANN Controller

Case 2: RCD control technique for Electric Spring with Conventional PI controller and ANN controller

In this part, three different values are selected for V_G to monitor its behavior when phase angle varies. Figure 9 shows the simulation results when phase sequence varies. In each subfigure, Two channels are recorded, reporting V_G, RMS value of the C_L voltage, respectively, phase angle, P_{in}, Pinref ,Reference Reactive powers by using PI and ANN controllers with comparisons has been shown.

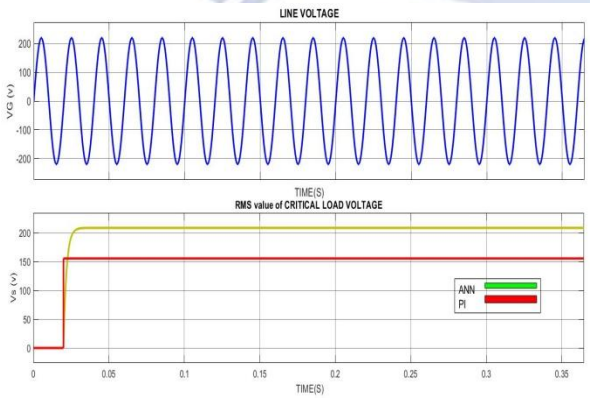

Figure 9: Simulation Waveform for input RMS value of Critical Voltage with PI and ANN Controller

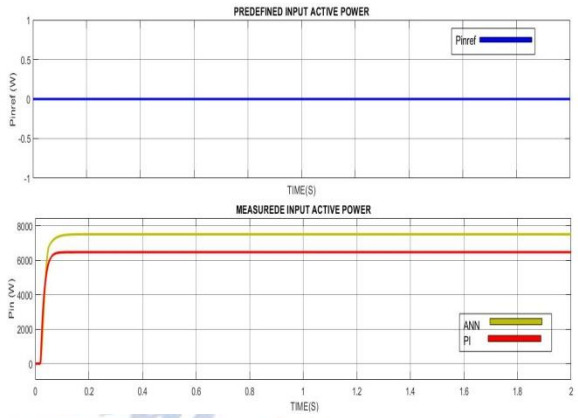

Figure 10: Simulation Waveform for Reference and Measured Active Powers with PI and ANN Controller

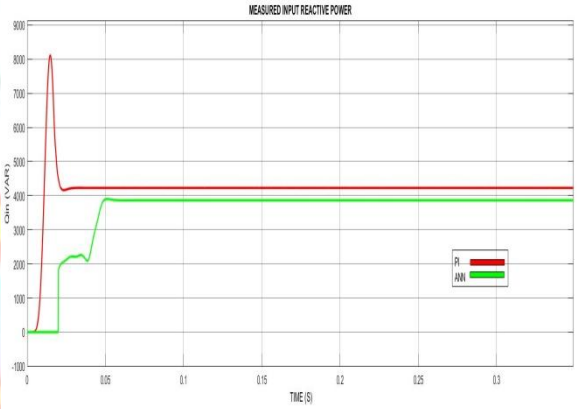

Figure 11: Simulation Waveform for Reactive powers of ES system with PI and ANN Controller

Case 3: Line Voltage variation for Electric Spring with Conventional PI controller and ANN controller

In this Subsection, the ES-2 transient responses to a change of V_G are monitored with P_{inref} fixed. They are traced in Figure 12. In each subfigure, four channels are recorded, reporting line voltage, reference value of the input active power, input active power and RMS value of C_L voltage, respectively, by using PI and ANN controllers with comparisons has been shown.

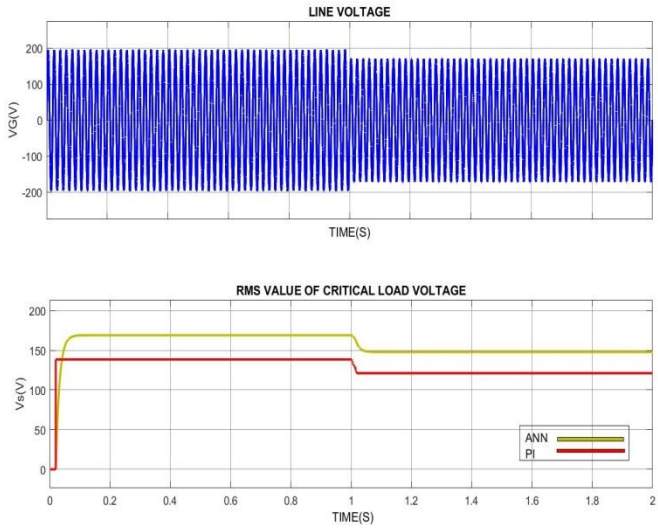

Figure 12: Simulation Waveform for RMS Critical Load Voltage with PI and ANN controller under Line Voltage Variation

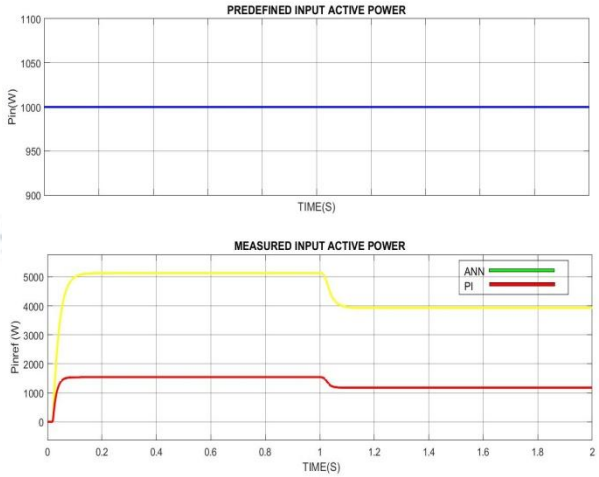

Figure 13: Simulation Waveform for measured Active Power of ES System with PI and ANN Controller

Figure 14: Simulation Waveform for measured Reactive Power of ES System with PI and ANN Controller

Case 4: A Simple PV system Application is adopted to Control the Grid Power and Voltage and to run the electric Spring-2 With a RCD Controller with ANN Technic.

In this final section, the ES-2 transient responses to a change of V_G are to monitored its behavior when phase angle varies. They are traced in Figure 15. In each subfigure, two channels are recorded, reporting line voltage, reference value of the input active power, input active power and RMS value of C_L voltage and reactive Power respectively. compared with by using PI and ANN Technic are shown.

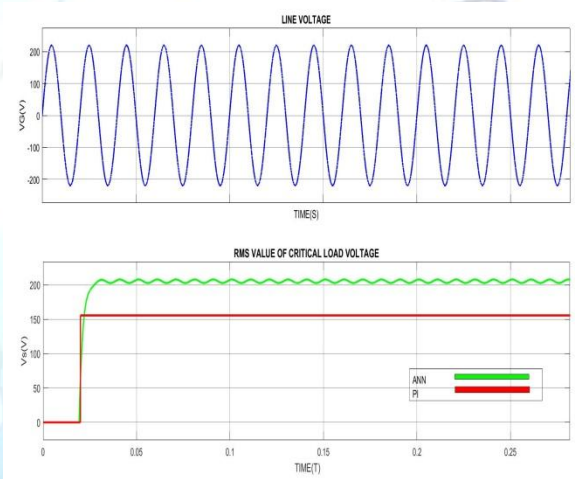

Figure 15: Simulation Waveform for RMS Critical Load Voltage with PI and ANN controller under Line Voltage Variation

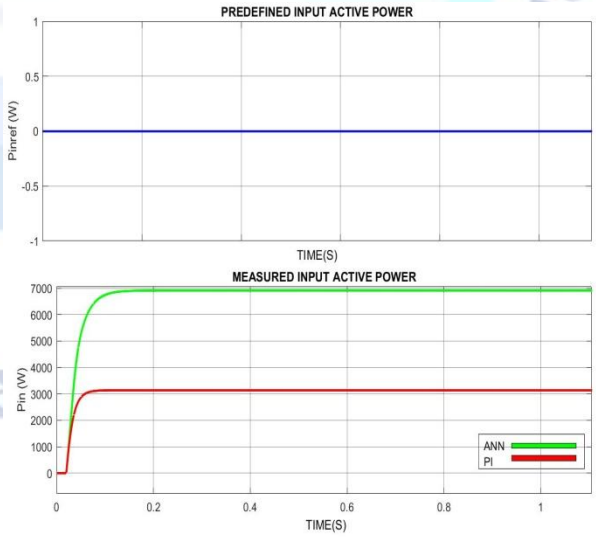

Figure 16: Simulation Waveform for measured Active Power of ES System with PI and ANN Controller

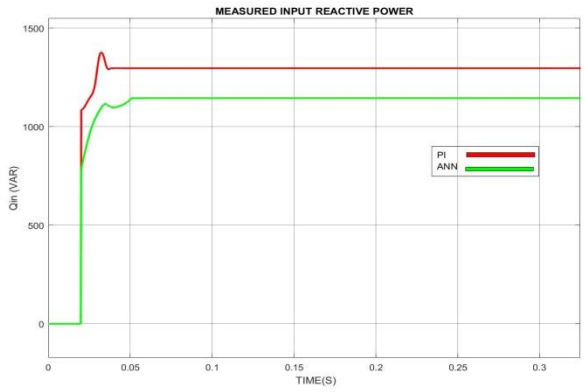

Figure 16: Simulation Waveform for measured Reactive Power of ES System with PI and ANN Controller.

5. CONCLUSION:

For the purpose of a practical application of ES-2, the input active and reactive power regulation is proposed with PI and ANN controllers in this paper. The controls on ES-2 are mostly used to control the input active power and reactive power, according to an overall assessment and analysis of the control systems now in use, including control and RCD control. The ES-2 is capable of handling the active power acquired by MPPT algorithm if it is outfitted with distributed generation from RESs. This implies that the ES-2 can manage the fluctuating power and ensure the controllable power to the grid. There have been simulations on the steady and transient analyses as well as under grid a normalizes, validating the efficacy of the proposed control. From these results the proposed ANN controller produces a better result as compared with conventional PI controller.

Conflict of interest statement

Authors declare that they do not have any conflict of interest.

REFERENCES

[1] Qingsong Wang, Senior Member, IEEE, Ming Cheng, Fellow, IEEE, Yun lei Jiang, Student Member, IEEE, Wujian Zuo, Giuseppe Buja, Life Fellow, IEEE.2017

[2] M. Cheng and Y. Zhu, "The state of the art of wind energy conversion systems and technologies: Areview," Energy Conversion and Management, vol. 88, pp. 332–347, Dec. 2014.

[3] P. Sotoodeh and R. D. Miller, "Design and implementation of an 11-level inverter with FACTS capability for distributed energy systems," IEEE J. Emerging Sel. Topics Power Electron., vol.2, no. 1, pp. 87–96, Mar. 2014.

[4] L. Wang, and D. N. Truong, "Stability enhancement of a power system with a PMSG-based and a DFIG-based offshore wind farm using a SVC With an adaptive-network-based fuzzy inference system," IEEE Trans. Ind. Electron., vol. 60, no. 7, pp. 2799–2807, Jul. 2013.

[5] Y. Zhang, X. Wu and X. Yuan, "A simplified branch and bound approach for model predictive control of multilevel cascaded H-bridge STATCOM," IEEE Trans. Ind. Electron., vol. 64, no. 10, pp. 7634–7644, Oct. 2017.

[6] W. Wang, L. Yan, X. Zeng, B. Fan, and J. M. Guerrero, "Principle and design of a single-phase inverter based grounding system for neutral-to-ground voltage compensation in distribution networks," IEEE Trans. Ind. Electron., vol. 64, no. 2, pp. 1204–1213, Feb. 2017.

[7] Q. Sun, J. Zhou, J. M. Guerrero, and H. Zhang, "Hybrid three-phase/single-phase microgrid architecture with power management capabilities," IEEE Trans. Power Electron., vol. 30, no. 10, pp. 5964– 5977, Oct. 2015.

[8] M. Andresen, G. Butichi, and M. Liserre, "Thermal stress analysis and MPPT optimization of photovoltaic systems," IEEE Trans. Ind. Electron., vol. 63, no. 8, pp. 4889–4898, Aug. 2016.

[9] F. Paz, and M. Ordonez, "High-performance solar MPPT using switching ripple identification based on a lock-in amplifier," IEEE Trans. Ind. Electron., vol. 63, no. 6, pp. 3595–3604, Jun. 2016.

[10] J. A. Munoz, J. R. Espinoza, C. R. Baier, L. A. Moran, E. E. Espinosa, P.

[11] Melin, and D. G. Sbarbaro, "Design of a discrete-time linear control strategy for a multicell UPQC," IEEE Trans. Ind. Electron., vol. 59, no. 10, pp. 3797–3807, Oct. 2012.

[12] S. Golestan, and J. M. Guerrero, "Conventional synchronous reference frame phase-locked loop is an adaptive complex filter," IEEE Trans. Ind. Electron., vol. 62, no. 3, pp. 1679–1682, Mar. 2015.